

# Intrinsic Domain and Loop Dynamics Commensurate with Catalytic Turnover in an Induced-Fit Enzyme

Omar Davulcu,<sup>1</sup> Peter F. Flynn,<sup>2</sup> Michael S. Chapman,<sup>1,\*</sup> and Jack J. Skalicky<sup>3,\*</sup>

<sup>1</sup>Department of Biochemistry and Molecular Biology, School of Medicine, Mail code L224, Oregon Health & Science University, 3181 Southwest Sam Jackson Park Road, Portland, OR 97239-3098, USA

<sup>2</sup>Department of Chemistry, University of Utah, 315 South 1400 East, Room 2020, Salt Lake City, Utah 84112-0850, USA

<sup>3</sup>Department of Biochemistry, University of Utah, 15 North Medical Drive East, Room 4100, Building 565, Salt Lake City, Utah 84112-5650, USA

\*Correspondence: [skalicky@biochem.utah.edu](mailto:skalicky@biochem.utah.edu) (J.J.S.), [chapmami@ohsu.edu](mailto:chapmami@ohsu.edu) (M.S.C.)

DOI 10.1016/j.str.2009.08.014

## SUMMARY

Arginine kinase catalyzes reversible phosphoryl transfer between ATP and arginine, buffering cellular ATP concentrations. Structures of substrate-free and -bound enzyme have highlighted a range of conformational changes thought to occur during the catalytic cycle. Here, NMR is used to characterize the intrinsic backbone dynamics over multiple time-scales. Relaxation dispersion indicates rigid-body motion of the N-terminal domain and flexible dynamics in the I182–G209 loop, both at millisecond rates commensurate with  $k_{\text{cat}}$ , implying that either might be rate limiting upon catalysis. Lipari-Szabo analysis indicates backbone flexibility on the nanosecond timescale in the V308–V322 loop, while the rest of the enzyme is more rigid in this timescale. Thus, intrinsic dynamics are most prominent in regions that have been independently implicated in conformational changes. Substrate-free enzyme may sample an ensemble of different conformations, of which a subset is selected upon substrate binding, with critical active site residues appropriately configured for binding and catalysis.

## INTRODUCTION

Arginine kinase (E.C. 2.7.3.3), a member of the phosphagen kinase family of enzymes, catalyzes reversible phosphoryl transfer between ATP and arginine, thus achieving cellular buffering of ATP levels in cells with high and/or variable energy demands (Ellington, 2001). It is chosen as a model for investigating enzyme dynamics due to its amenability to both high resolution crystallography and nuclear magnetic resonance (NMR) spectroscopy.

The phosphagen kinase family of enzymes has been the focus of a large body of research resulting in significant advances in our understanding of bimolecular enzyme catalysis (Ellington, 2001). Steady-state enzyme kinetics have shown that arginine kinase undergoes a rapid equilibrium, random order bimolecular-bimolecular reaction, likely common to all phosphagen kinases, with a turnover number ( $k_{\text{cat}}$ ) in the range of 100 to 150  $\text{s}^{-1}$  (Blethen, 1972; Gattis et al., 2004; Pruet et al., 2003).

X-ray solution scattering experiments, which detected a decrease in the radius of gyration of arginine kinase upon substrate binding, were the first to indicate that substrate binding is accompanied by large conformational changes and raised the possibility that the change could be rate limiting (Dumas and Janin, 1983).

X-ray crystal structures have provided the clearest view of the extent of conformational changes in *Limulus polyphemus* arginine kinase. Two structures of arginine kinase are available: one in a substrate-free, or “open,” form at 2.4 Å resolution and one in a transition state analog complex, substrate-bound or “closed,” form at 1.2 Å resolution (Yousef et al., 2003, 2002; Zhou et al., 1998). These structures show arginine kinase to be a monomeric, two domain enzyme with a small,  $\alpha$ -helical N-terminal domain (NTD) linked to a larger, primarily  $\beta$  sheet C-terminal domain (CTD), with substrates binding in the cleft between these two domains. In the substrate-bound form, both NTDs and CTDs fold over the active site, along with a number of loops, analogous to a hand making a grabbing motion (Yousef et al., 2003).

Over the last decade, the concept of “dynamic domain” has been used increasingly to describe clusters of atoms whose conformational change can be approximated to a common rotation/translation operator (Gerstein et al., 1994; Hayward, 1999; Hayward and Berendsen, 1998; Lee et al., 2003). A dynamic domain may include noncontiguous regions of linear sequence, so dynamic domains are an extension of the classical definition of domains as globular and linearly contiguous units. Analysis of substrate-free and transition state arginine kinase show the conformational differences can be approximated as rotations of three dynamic domains by up to 18° relative to a fixed domain with additional loop reconfigurations overlaid that bring catalytically important residues to the active site (Yousef et al., 2003). These changes may be involved in mediating substrate specificity, preventing wasteful hydrolysis of ATP, and precisely aligning substrates for phosphoryl transfer (Jencks, 1969, 1975; Jencks and Mage, 1974; Lahiri et al., 2002).

There is growing evidence that enzymes bind substrates with a “conformational selection” mechanism (Boehr et al., 2006; Boehr and Wright, 2008; Lange et al., 2008; Ma et al., 1999). In the absence of substrate, an equilibrium may exist between substrate-free states and ones that are closer to the substrate-bound conformation. Binding of substrates stabilizes the ligand-bound state, shifting the preexisting equilibrium toward the

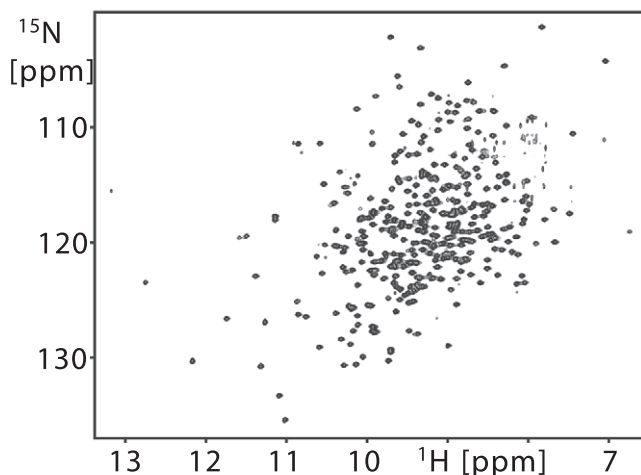


**Figure 1. 2D [ $^{15}\text{N}$ , $^1\text{H}$ ] TROSY of Arginine Kinase Recorded at 800 MHz for the Shortest  $T_1$  Delay Measurement**

The average signal-to-noise ratio of signals from the shortest relaxation delay time of  $T_1$  and  $T_{1\text{rho}}$  measurement are 165/1 and 181/1 at 50.65 MHz, 202/1 and 200/1 at 60.78 MHz, and 370/1 and 250/1 at 81.04 MHz. The average signal-to-noise ratio from the  $\{^1\text{H}\}^{15}\text{N}$  NOE reference spectrum is 165/1.

ligand-bound form. Enzyme-substrate interactions in an ATP binding cassette (Wang et al., 2004), RNase A (Beach et al., 2005; Kovrigin and Loria, 2006), dihydrofolate reductase (Osborne et al., 2001), and other enzymes (Boehr et al., 2006), as well as antibody-antigen interactions (Bosshard, 2001), have been explained in terms of conformational selection. Conformational selection embodies statistical mechanics, in subtle contrast to Koshland's deterministic view of induced fit, where the bound configuration is only attained when the enzyme binds a substrate molecule (Koshland, 1958, 1994). The two mechanistic models represent extremes on a continuum and there may be elements of both in the same system. Thus an excited state sampled via conformational selection may move closer to the ligand-bound state, but a substrate-initiated change may be needed to attain the final substrate-bound configuration (Sullivan and Holyoak, 2008). In this paper, we examine the timescales of backbone dynamics of an enzyme in the absence of substrates and correlate these findings with the structural changes and kinetics of enzyme turnover that occur in the presence of substrates.

## RESULTS

NMR  $^{15}\text{N}$  relaxation rate constants were measured for 303 of the 344 nonproline backbone amides in substrate-free arginine kinase. This included all assigned nonoverlapping resonances (Davulcu et al., 2005). The NMR data are of high quality as illustrated by a 2D [ $^{15}\text{N}$ , $^1\text{H}$ ] TROSY spectrum of the enzyme (Figure 1). All relaxation rate constant measurements were detected on the slow relaxing spin transition using [ $^{15}\text{N}$ , $^1\text{H}$ ] TROSY detection schemes.

### Slow ( $\mu\text{s}$ -ms) Timescale Dynamics

We began this study with a focus on identifying arginine kinase residues that exhibit  $\mu\text{s}$ -ms timescale motion. Main chain

dynamics on this timescale were measured using two independent experimental approaches. First,  $^{15}\text{N}$  relaxation dispersion identified 34 residues with  $R_{\text{ex}} > 2 \text{ s}^{-1}$  (Table 1). Representative  $^{15}\text{N}$  relaxation dispersion data at three static field strengths are shown in Figure 2. Second, independent  $R_{\text{ex}}$  measurements from a complementary NMR relaxation experiment identified 17 residues with  $R_{\text{ex}}$  above a conservative threshold of  $5 \text{ s}^{-1}$  (Figure 3 and Table 1) of which just F136 had not previously been identified (Wang et al., 2003). Thus, we identified a total of 35 residues with relaxation arising from chemical exchange ( $R_{\text{ex}}$ ) representing at least 12% of the protein.

Residues with  $R_{\text{ex}}$  are prevalent at four prominent locations in the protein (Figures 3 and 4 and Table 1): (1) D88–G92, within a hinge linking the NTDs and CTDs; (2) D71, F136–N137, F270–G276, and G332, which all lie at the interface between the NTDs and CTDs; (3) R126–L131 and V220–Q234, which largely constitute the hinges of dynamic domains 1 and 2; and (4) I182–G209, a substrate binding loop.

Resonances showing chemical exchange were fit to the Bloch-McConnell equation, and assuming two-state exchange, estimates of  $k_{\text{ex}}$ , populations  $p_A$  and  $p_B$ , and the chemical shift difference between states A and B ( $\Delta\omega$ ) were obtained (Cavanagh et al., 1996; Palmer et al., 2001). Representative  $^{15}\text{N}$  spin relaxation dispersion curves are shown in Figure 2 and their fit exchange parameters are listed in Table 1. Conformational exchange rate constants,  $k_{\text{ex}}$ , of individual residues range from 400 to  $4200 \text{ s}^{-1}$  with significantly skewed  $p_A/p_B$  ratios. The fit  $^{15}\text{N}$  chemical shift difference,  $\Delta\omega$ , ranges from 0.8 to 5.6 ppm. Analysis for a small number of residues did not converge, likely the result of small  $R_{\text{ex}}$ . Dispersion data from residues in spatially distinct locations of the enzyme were fit together assuming they share a common motion responsible for the chemical exchange with the same  $k_{\text{ex}}$  and relative populations  $p_A$  and  $p_B$ . The groupings and fit parameters are listed in Table 1. Further attempts to consolidate by fitting common parameters dynamic domain 1, its hinge, and flexible loop L8 were unsuccessful.

### Fast (ns-ps) Timescale Dynamics

NMR spin relaxation measurements were recorded at three static field strengths,  $^{15}\text{N}$   $\omega_0 = 50.65$ , 60.78, and 81.04 MHz, and analyzed with the Lipari-Szabo model-free approach or extended model-free, providing ns-ps dynamics information (Clare et al., 1990; Lipari and Szabo, 1982a, 1982b).  $^{15}\text{N}$  spin longitudinal ( $T_1$ ) and transverse ( $T_2$ ) relaxation time constants were measured at each field and the heteronuclear  $\{^1\text{H}\}^{15}\text{N}$  nuclear Overhauser effect (NOE) measured at 60.78 MHz only, yielding a total of seven measurements per residue. The data were recorded with high signal to noise ratio (Figure 1), resulting in reliable  $T_1$ ,  $T_2$ , and NOE values with most standard deviations  $< 2\%$ . The relaxation time constants and NOE values are plotted in Figure 5 and listed in Table S1 (available online). Mean and “trimmed” mean values, the subset used in the isotropic  $\tau_m$  calculation, are listed in Table 2. The theoretical maximum NOE, in the rigid limit and  $\tau_m = 23 \text{ ns}$ , is 0.83 and only two residues are larger by more than two standard deviations, T269 and L333.

NMR spin relaxation measurements were fit to isotropic and axial-symmetric anisotropic rotational diffusion models using established methods (Tjandra et al., 1995a). Evidence derived from

**Table 1. Summary of Two-State Exchange Parameters for Individual and Groups of Residues in Substrate-Free Arginine Kinase**

	Residue	2°	Individual Fits			Collective Fits		
			$k_{\text{ex}}$ (s <sup>-1</sup> )	$p_B$ (%)	$ \Delta\omega $ (ppm)	$k_{\text{ex}}$ (s <sup>-1</sup> )	$p_B$ (%)	$ \Delta\omega $ (ppm)
NTD hinge	D88	$\alpha 4$	3200 ± 240	0.3 ± 0.1	1.9 ± 0.3	1930 ± 350	0.4 ± 0.1	3.2 ± 0.3
	H90	$\alpha 4$	1020 ± 480	0.4 ± 0.1	4.5 ± 0.5			4.4 ± 0.6
	G92	L4	1560 ± 760	0.3 ± 0.1	5.1 ± 0.6			3.4 ± 0.4
NTD-CTD interface	D71	L3	*	*	*	800 ± 100	1.1 ± 0.1	1.1 ± 0.1
	F136	L6						
	N137	L6	1150 ± 160	1.9 ± 0.7	0.9 ± 0.6			1.7 ± 0.2
	F270	L11	2830 ± 230	0.9 ± 0.8	2.3 ± 0.5			2.4 ± 0.4
	C271	L11	*	*	*			0.9 ± 0.3
	N274	L11	1100 ± 710	0.6 ± 0.1	3.6 ± 0.7			1.6 ± 0.2
	G276	L11	1930 ± 340	1.4 ± 0.4	3.0 ± 0.6			3.8 ± 0.5
	G332	L14	1330 ± 320	1.5 ± 2.1	1.5 ± 1.0			1.5 ± 0.1
Dynamic domain 1 and hinge	R126	$\beta 1$	690 ± 220	0.3 ± 0.1	2.9 ± 0.3	790 ± 70	0.4 ± 0.1	2.2 ± 0.3
	C127	$\beta 1$	940 ± 550	0.2 ± 0.1	3.7 ± 0.6			1.9 ± 2.3
	R129	$\beta 1$	950 ± 450	0.3 ± 0.1	5.6 ± 0.4			5.6 ± 0.2
	V220	$\beta 4$	2360 ± 210	1.0 ± 0.1	1.3 ± 0.1			2.7 ± 3.0
	V222	$\beta 4$	*	*	*			1.7 ± 0.6
	R229	$\beta 5$	360 ± 350	0.3 ± 0.2	2.5 ± 0.4			1.7 ± 0.1
	Q234	$\beta 5$	*	*	*			1.0 ± 1.0
Substrate binding loop L8	I182	$\alpha 7$	700 ± 420	0.5 ± 0.2	4.5 ± 0.4	790 ± 60	2.6 ± 0.6	0.8 ± 0.4
	D183	$\alpha 7$	*	*	*			*
	D184	$\alpha 7$	2730 ± 1760	0.5 ± 1.3	3.1 ± 4.5			0.6 ± 0.3
	H185	$\alpha 7$	1810 ± 650	0.3 ± 0.1	5.1 ± 0.6			0.8 ± 0.4
	E190	L8	990 ± 70	4.5 ± 0.6	1.6 ± 0.1			2.4 ± 0.8
	G191	L8	*	*	*			*
	D192	L8	760 ± 90	1.7 ± 0.4	1.3 ± 0.2			1.0 ± 0.2
	R193	L8	1470 ± 390	0.5 ± 0.1	4.4 ± 0.4			1.0 ± 0.5
	T197	L8	3660 ± 1360	0.5 ± 0.1	6.8 ± 1.3			1.1 ± 0.9
	A198	L8	4190 ± 1160	0.0 ± 1.2	2.6 ± 1.6			*
	A200	L8	1610 ± 440	0.7 ± 0.1	4.6 ± 0.5			1.3 ± 0.7
	C201	L8	510 ± 230	1.3 ± 0.1	1.9 ± 0.3			1.2 ± 0.1
	R202	L8	1300 ± 220	0.0 ± 0.0	0.8 ± 0.1			0.8 ± 0.6
	T206	L8	570 ± 50	2.6 ± 0.2	1.7 ± 0.1			1.7 ± 0.2
	G207	L8	1350 ± 140	0.0 ± 0.0	0.8 ± 0.1			0.7 ± 0.3
	R208	L8	920 ± 180	0.6 ± 0.1	3.8 ± 0.2			1.1 ± 0.1
G209	$\beta 3$	1450 ± 380	0.7 ± 0.2	3.3 ± 0.6	1.1 ± 0.2			

Secondary structure of each residue is denoted with 2° as observed in the substrate-free crystal structure of arginine kinase. In all cases, fitting was performed assuming a two-state exchange model, where  $k_{\text{ex}}$  is the sum of forward and reverse rate constants,  $p_B$  is the relative population of the higher energy state, and  $\Delta\omega$  is the chemical shift difference between the two states. Asterisks denote residues for which fitting did not converge.

calculation and experiment strongly suggests that the axial-symmetric diffusion model is more appropriate. First, calculation of rotational diffusion anisotropy from NMR data with the substrate-free arginine kinase coordinates, assuming axial symmetric diffusion, resulted in a ratio of rotational diffusion rate constants,  $D_{\text{par}}/D_{\text{perp}}$  of 0.86, which corresponds to an oblate ellipsoid (Yousef et al., 2003). The final diffusion tensor for 1M80.pdb was  $D_{\text{par}} = 6.50 \times 10^6 \text{ s}^{-1}$ ,  $D_{\text{perp}} = 7.54 \times 10^6 \text{ s}^{-1}$ ,  $\theta = 1.62 \text{ rad}$ , and  $\phi = 0.72 \text{ rad}$ . Second, the calculated ratio of rotational diffusion rate constants for substrate-free arginine kinase using HYDRONMR was 0.80, consistent with the experi-

mental results (Garcia de la Torre et al., 2000; Yousef et al., 2003). Finally, the consensus optimal value of  $\tau_m$  and the average value of  $\tau_m$  for the amide resonances of the individual residues fit to isotropic models both indicate that the value of the rotational correlation time is 23 ns. In contrast, the  $\tau_m$  values for the amide nuclei in individual range between 21.0 and 25.7 ns, which is inconsistent with isotropic diffusion, but consistent with data acquired for a system that exhibits anisotropic rotational diffusion but fit to an isotropic model. We therefore proceed with subsequent analysis of the NMR relaxation data using an anisotropic model.

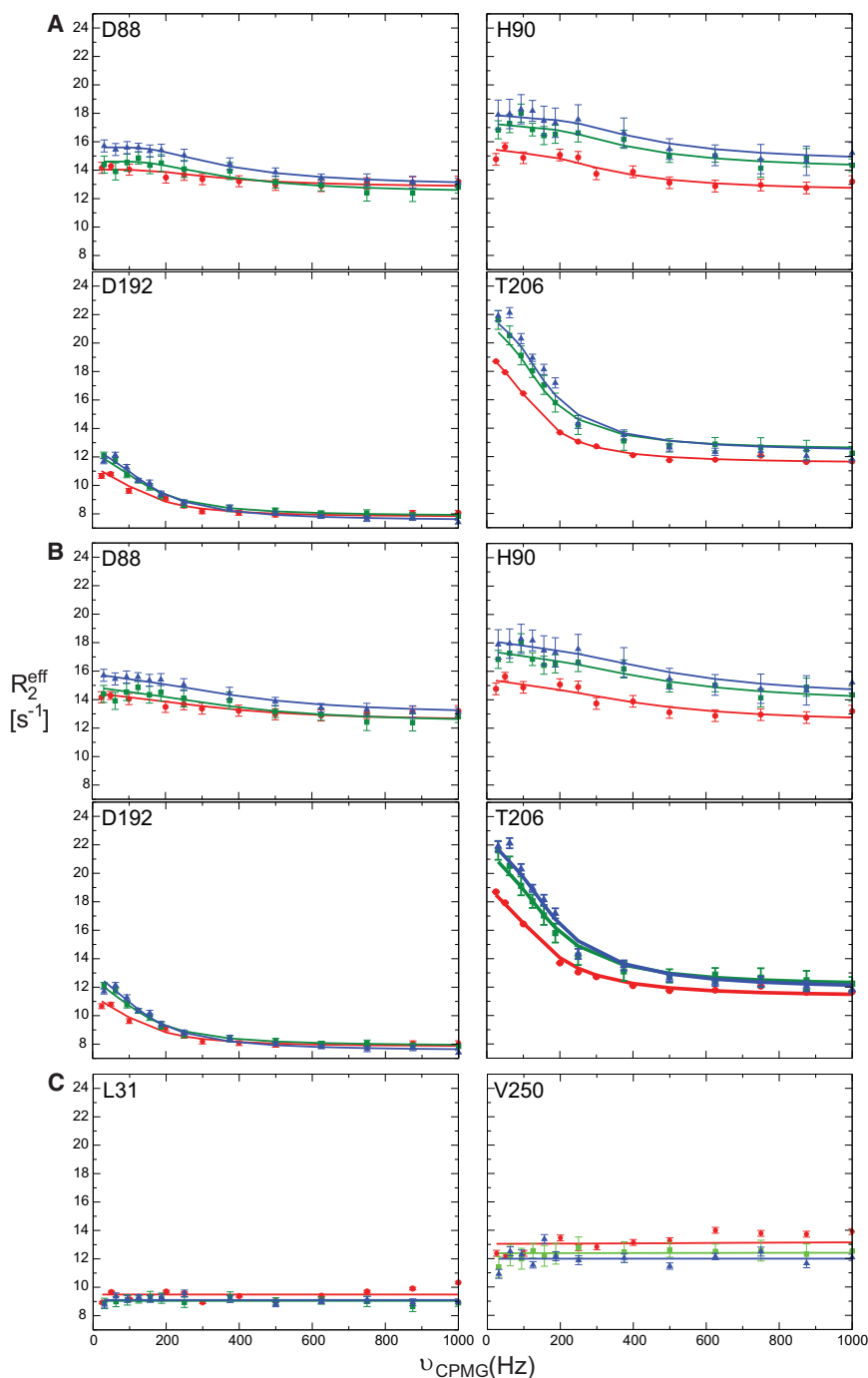


**Figure 2.  $^{15}\text{N}$  Spin Relaxation Dispersion Curves for Selected Residues with  $\mu\text{s}$ -ms Timescale Dynamics: D88, H90, D192, and T206**

(A) Individual fit dispersion curves at  $^{15}\text{N}$  Larmor frequencies 60.78 (red circles), 72.05 (green squares), and 81.04 MHz (blue triangles).

(B) Collective fit dispersion curves for the same residues: D88 and H90 with G92 and D192 and T206 with 12 other residues (Table 1).

(C)  $^{15}\text{N}$  spin relaxation dispersion curves for residues with no  $R_{\text{ex}}$ . Errors were determined from duplicate measurements of  $R_2^{\text{eff}}$ .

model. Model selection results are summarized in Table 3. About 35% of the residues were best fit using models 3 and 4, indicating even more extensive  $\mu\text{s}$ -ms chemical exchange (Figure 6) than reported by relaxation dispersion. Alternative analysis using an isotropic diffusion model indicates a slightly higher fraction (40%) of residues best fit to models 3 and 4 (data not shown). About 14% of the residues (43) were best fit to model 5 ( $S^2$ ,  $S^2_{\text{tr}}$ ,  $S^2_{\text{ss}}$ ,  $\tau_{\text{s}}$ ) and are most abundant in loops and turns. Most residues best fit with model 5 have a slow time constant,  $\text{ave}_{\tau_{\text{s}}} = 1 \pm 0.4$  ns. It should be appreciated that the error in estimating the local correlation time is larger than that of other fitted parameters. Furthermore, in the current analysis, a single measurement of the  $\{^1\text{H}\}^{15}\text{N}$  NOE was used that decreases the precision of the estimate somewhat. Although the  $\tau_{\text{s}}$  values are relatively large, because  $\tau_{\text{m}}$  is also large (23 ns), the Lipari-Szabo decoupling approximation is not violated (Lipari and Szabo, 1982a, 1982b; Vugmeyster et al., 2003). Nearly all residues best fit to model 2 ( $S^2$ ,  $\tau_{\text{e}}$ ) and 4 ( $S^2$ ,  $\tau_{\text{e}}$ ,  $R_{\text{ex}}$ ) have  $\tau_{\text{e}}$  values  $< 20$  ps. The  $\text{ave}S^2$  over all residues is  $0.85 \pm 0.06$  and is significantly lower only for residues in loops L1, L12, and L13 (Figure 6 and Table S2). Overall, the enzyme is relatively rigid on the ns-ps timescale with the exception of three

Following standard procedures and using axial symmetric diffusion, the ns-ps dynamics of each residue was analyzed and reported in Figure 6 and listed in Table S2 (Clarkson et al., 2006; d'Auvergne and Gooley, 2003; Mandel et al., 1995). Model selection was guided by the  $\chi^2$  error. Where  $\chi^2$  could not distinguish two or more models, the simplest was chosen. Models 3 ( $S^2$ ,  $R_{\text{ex}}$ ) and 4 ( $S^2$ ,  $\tau_{\text{e}}$ ,  $R_{\text{ex}}$ ) were excluded if the fit  $R_{\text{ex}}$  was  $< 1$   $\text{s}^{-1}$ . This cutoff was chosen since the experimental error of  $R_2$  is about 1  $\text{s}^{-1}$ . Residues V308–V322, which are absent in the PDB coordinates, were necessarily fit using the isotropic

loops, including one, loop L13, which has previously been shown to be crucial for substrate binding.

## DISCUSSION

Interpretation of the main chain dynamics will be discussed with reference to classical as well as “dynamic” domain structure; dynamic domains being more appropriate in describing the differences between substrate-free and -bound crystal structures. This is not to imply that the intrinsic dynamics observed



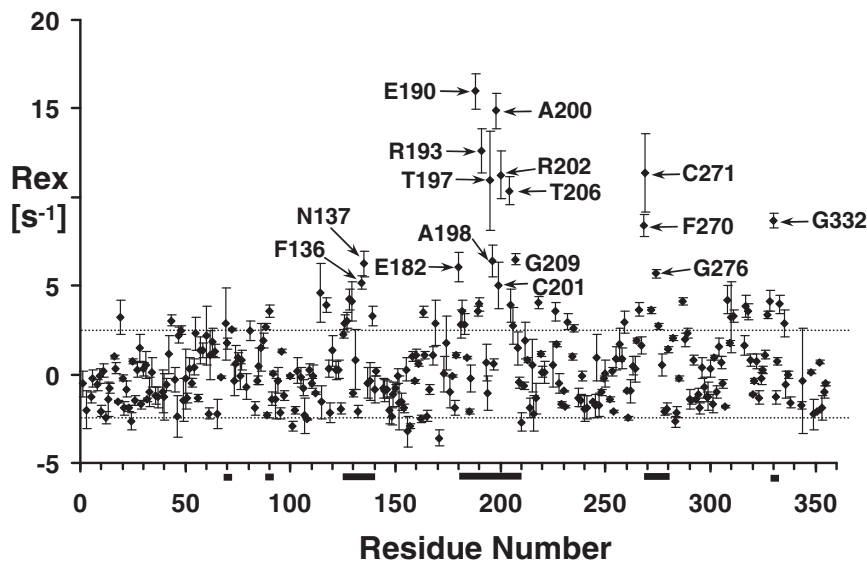


**Figure 3. Chemical Exchange in Substrate-Free Arginine Kinase Identified from  $R_{ex} = R_2^\beta - R_1^{2HzNz}/2 - \eta_{xy}(\kappa - 1) + R_1N/2$**

$\kappa =$  trimmed mean of  $1 + (R_2^\beta \times R_1^{2HzNz}/2)/\eta_{xy} = 1.43$ . For apparently nonexchanging residues, the average  $R_{ex}$  is  $0.05 \pm 2.5 \text{ s}^{-1}$ ; error is shown with dashed lines. The large error is partly due to residue-specific variation in the  $^{15}\text{N}$  CSA tensor magnitude and orientation. The solid bars represent polypeptide segments having residues with  $^{15}\text{N}$  spin relaxation dispersion. Error bars are from measurements in triplicate. Residues with  $R_{ex}$  greater than two standard deviations ( $5 \text{ s}^{-1}$ ) are labeled.

by NMR in substrate-free form must necessarily be of the same magnitude or direction as the large conformational changes revealed in the substrate-bound crystallographic structures. Furthermore, NMR can reveal motions between open and closed states, some of which may be populated at levels too low to be detectable crystallographically. Despite these caveats, there is good correspondence between the locations of residues exhibiting chemical change or increased flexibility and prediction based on the crystal structures.

The classical description of arginine kinase is as two domains: a small,  $\alpha$ -helical NTD spanning residues 1–90 and a larger, primarily  $\beta$  sheet CTD spanning residues 120–357, with the active site lying in the cleft between these domains. The domains are connected with residues 91–119, a region well defined by crystallography but lacking regular  $\alpha$ -helical or  $\beta$  strand structure. Upon binding substrates, the two domains close over the active site. Closing of the two domains positions several substrate-binding and catalytically important residues in the active site, underlying the importance of dynamics on turnover of the enzyme (Yousef et al., 2003; Zhou et al., 1998).

Arginine kinase can also be described as three dynamic domains that rotate independently relative to a fourth, fixed domain (Yousef et al., 2003). The overall structure of dynamic domains is shown in Figures 4A and 4B and compared to classical domains in Figures 4C–4F. Dynamic domain 1 is an extended and larger version of the NTD, while dynamic domains 2 and 3 are primarily large loops (L8 and L13) of the classical CTD.

#### Rigid Body Motion of the N-terminal Domain

Between the substrate-free and -bound states, the (classical) NTD of arginine kinase undergoes a significant rigid-body motion—a hinged rotation of the domain about residues 88–94 (Figures 4A and 4B) (Yousef et al., 2003; Zhou et al., 1998). Domain rotation also causes a flexing at the NTD-CTD interface (Figure 4). The open and closed forms of the enzyme show little difference in the internal structure of the NTD. The average

CTD also shows sizeable differences between the open and closed form crystal structures at residues 92–94, with composite torsion angle changes of  $15^\circ$ ,  $18^\circ$ , and  $29^\circ$  (Yousef et al., 2003; Zhou et al., 1998).

NMR relaxation dispersion identifies  $\mu\text{s}$ – $\text{ms}$  timescale motion for multiple residues in the hinge and interface (Figures 4E and 4F). Their distribution is consistent with a rigid body motion with little change in internal structure: the NTD core is devoid of  $R_{ex}$  with the exception of D71, located in the interface with the CTD (Figure 4). Assuming two-state exchange between open and closed forms, we fit exchange parameters for individual residues and groups with the Bloch-McConnell equation (Table 1). Fitting NMR relaxation dispersion for three individual hinge residues (D88, G90, and G92) resulted in similar  $k_{ex}$  and  $p_B$  values, while fitting a single collective motion yields  $k_{ex} = 1930 \pm 350 \text{ s}^{-1}$  and  $p_B = 0.4 \pm 0.1\%$ . The equilibrium is highly skewed; the approximate  $k_{open}$  and  $k_{close}$  rate constants are  $1920$  and  $10 \text{ s}^{-1}$ , respectively. For eight NTD-CTD interface residues (D71, F136, N137, F270, C271, N274, G276, and G332) individual  $k_{ex}$  values range from  $1200$  to  $2800 \text{ s}^{-1}$  with skewed populations and  $p_B < 2\%$ , while a collective fit yields  $k_{ex} = 800 \pm 100 \text{ s}^{-1}$  and  $p_B = 1.1 \pm 0.1\%$  (Table 1). Estimates of  $k_{open}$  and  $k_{close}$  are  $790 \text{ s}^{-1}$  and  $10 \text{ s}^{-1}$ , respectively. The collective interface  $k_{ex}$  is about half that of the hinge. We note that the hinge and interface residues fit small relative population  $p_B$ , which can lead to uncertainty in the exact parameter values fit. A collective fit of hinge and interface residues together was unsuccessful. In summary, the hinge and interface residues exhibit  $\mu\text{s}$ – $\text{ms}$  timescale dynamics, with a highly skewed equilibrium  $p_B \approx 1\%$ ,  $k_{open} \approx 790$ – $1920 \text{ s}^{-1}$ , and  $k_{close} \approx 10 \text{ s}^{-1}$ . The slower of the two rate constants is of the same order as  $k_{cat}$  and potentially rate limiting.

Additional residues exhibiting  $R_{ex}$  can be understood with the dynamic domain model (Figures 4A and 4B; Zhou et al., 1998; Yousef et al., 2003). R126, C127, R129, V220, V222, R229, and Q234 are located in the 49 residue dynamic domain 1 hinge or near the bottoms of the substrate binding pockets (Figure 4;

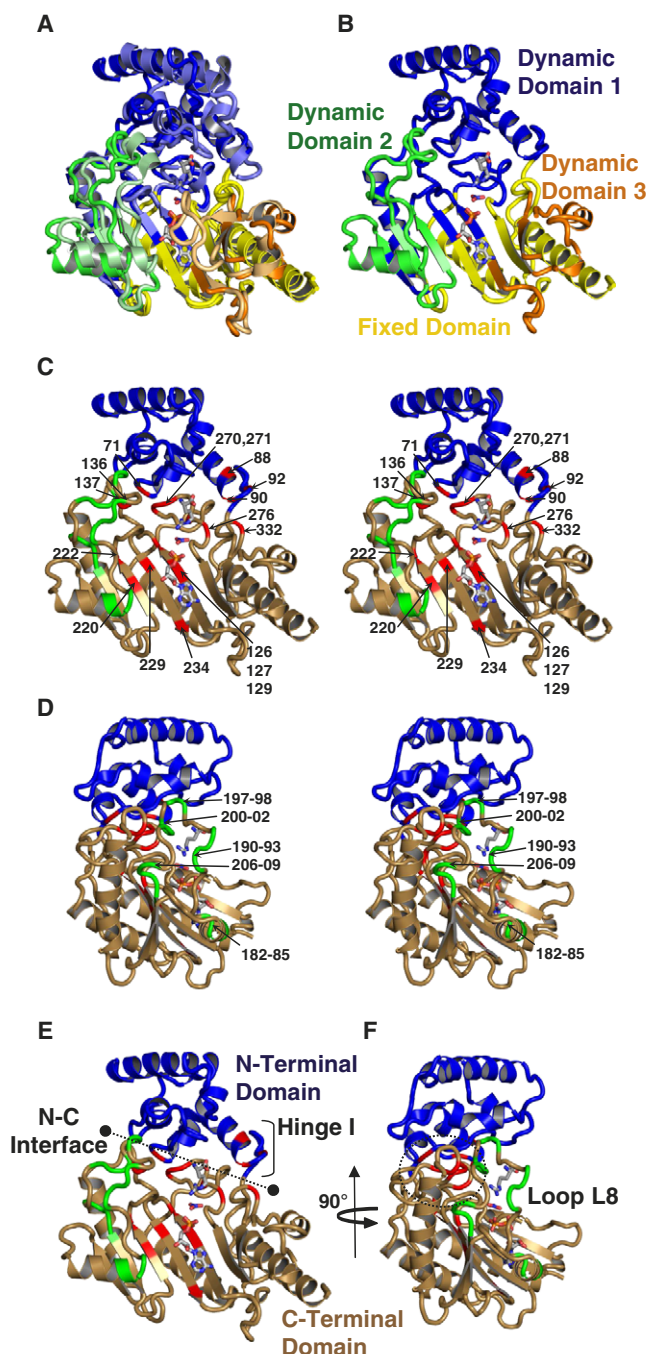


**Figure 4. Conformational Dynamics of Arginine Kinase**

(A) Comparison of the dynamic domains of substrate-free and -bound structures of arginine kinase (Yousef et al., 2003; Zhou et al., 1998). Dynamic domains 1, 2, and 3 are colored, respectively, blue, green, and orange. The darker shade of each color is substrate-free and fixed domain is shown in yellow.

(B) Only substrate free.

(C–F) Amino acids with measurable  $R_{ex}$ , colored red, with the exception of residues between 180 and 209, near L8, which are shown in green. The classical NTDs and CTDs are shown blue and sand. C and D are stereographic pairs with loop 8 residues labeled in D and all others labeled in C. D and F are rotated 90° with respect to C and E.

(E) The interface between NTDs and CTDs and location of NTD hinge.

In all panels, substrates ADP,  $\text{NO}_3^-$  anion, and arginine are shown from the substrate-bound structure to guide the eye.

Yousef et al., 2003). A collective fit for all dynamic domain 1 and hinge residues results in a reasonable  $k_{ex}$  ( $990 \pm 110 \text{ s}^{-1}$ ) but very small  $p_B$  ( $<0.3\%$ ) and unreasonably large  $\Delta\omega$  and errors (data not shown). Of significant importance for enzyme function, movement of the NTD helps position the substrate specificity loop L3, L61–A72, to coordinate substrate arginine (Suzuki et al., 1997). Additionally, conserved residues C271 and N223–H227 move as part of dynamic domain 1 and have been shown to be important for catalysis and substrate binding (Furter et al., 1993; Zhou et al., 1998). Thus, even if only semiquantitatively, NMR confirms  $\mu\text{s}$ – $\text{ms}$  timescale dynamics of the NTD (or dynamic domain 1 and hinge 1) and demonstrates that the motions are intrinsic to substrate-free arginine kinase and not just substrate gated.

On the ps–ns timescale, the entirety of the classical NTD or dynamic domain 1 and hinges are mostly rigid, with only a few locations showing increased flexibility ( $S^2 < 0.8$ ). The average order parameter,  $S^2$ , for the NTD is  $0.85 \pm 0.04$ , and of the NTD loops, only L1 (residues S21–K24) shows significantly lower  $S^2$  values while L2 (N41–T49), and L3 (L61–A72) reveal only slightly below average  $S^2$  (Table S2 and Figure 6). Loop L1 is surface exposed and distant from the active site. The average  $S^2$  of hinge residues is similar to the average of the NTD residues. Loop L4 (G91–G105) of the NTD-CTD linker and loops L6 (S130–L140) and L11 (K256–M279) at the NTD-CTD interface also show very small decreases in  $S^2$ , indicating some increased local flexibility.

#### Dynamics of Substrate Binding Loop L8 (I182–G209)

Substrate binding loop L8 changes conformation between open and closed structures to help close the entrance to the nucleotide binding site (Yousef et al., 2003; Zhou et al., 1998). The overall displacement of L8 is 5.4 Å, but internal to L8, the rmsd is only 1.4 Å (Figure 4). The average composite torsion angle change in loop L8 between open and closed forms of arginine kinase is 36°. Similar to the NTD, loop L8 has characteristics of a rigid body motion, but the larger composite torsion angle change and rmsd suggest a more complex motional model.

NMR relaxation dispersion shows a high fraction (60%) of loop L8 residues with  $R_{ex}$ . Fitting dispersion for individual residues yields a range of  $k_{ex}$  from 500 to 2700  $\text{s}^{-1}$  and skewed populations,  $p_B < 4.5\%$ ; a collective fit of all seventeen residues yields  $k_{ex} = 790 \pm 60 \text{ s}^{-1}$ ,  $p_B = 2.6 \pm 0.6\%$ ,  $k_{open} \approx 770 \text{ s}^{-1}$ , and  $k_{close} \approx 20 \text{ s}^{-1}$  (Table 1) and assumes the predominant conformer is the open state. The smaller of the two rate constants is on the same order as  $k_{cat}$ .

NMR confirms that  $\mu\text{s}$ – $\text{ms}$  timescale dynamics in loop L8 are intrinsic to substrate-free arginine kinase and not only substrate gated. Backbone crystallographic B factors for this loop in the structure of the unbound protein are elevated about two-fold. In contrast, B factors for loop L8 in the substrate-bound form are not elevated, indicating relative ordering compared to the substrate-free structure. Overall, the NMR results are consistent with substrate nucleotide binding. The closed structure of the enzyme places loop L8 residue H185, along with H284, in a stacked arrangement with the purine ring of substrate ADP (Zhou et al., 1998). We thus speculate that the intrinsic motion present in loop L8 may sample the closed-form configuration, which is then selected with nucleotide binding.

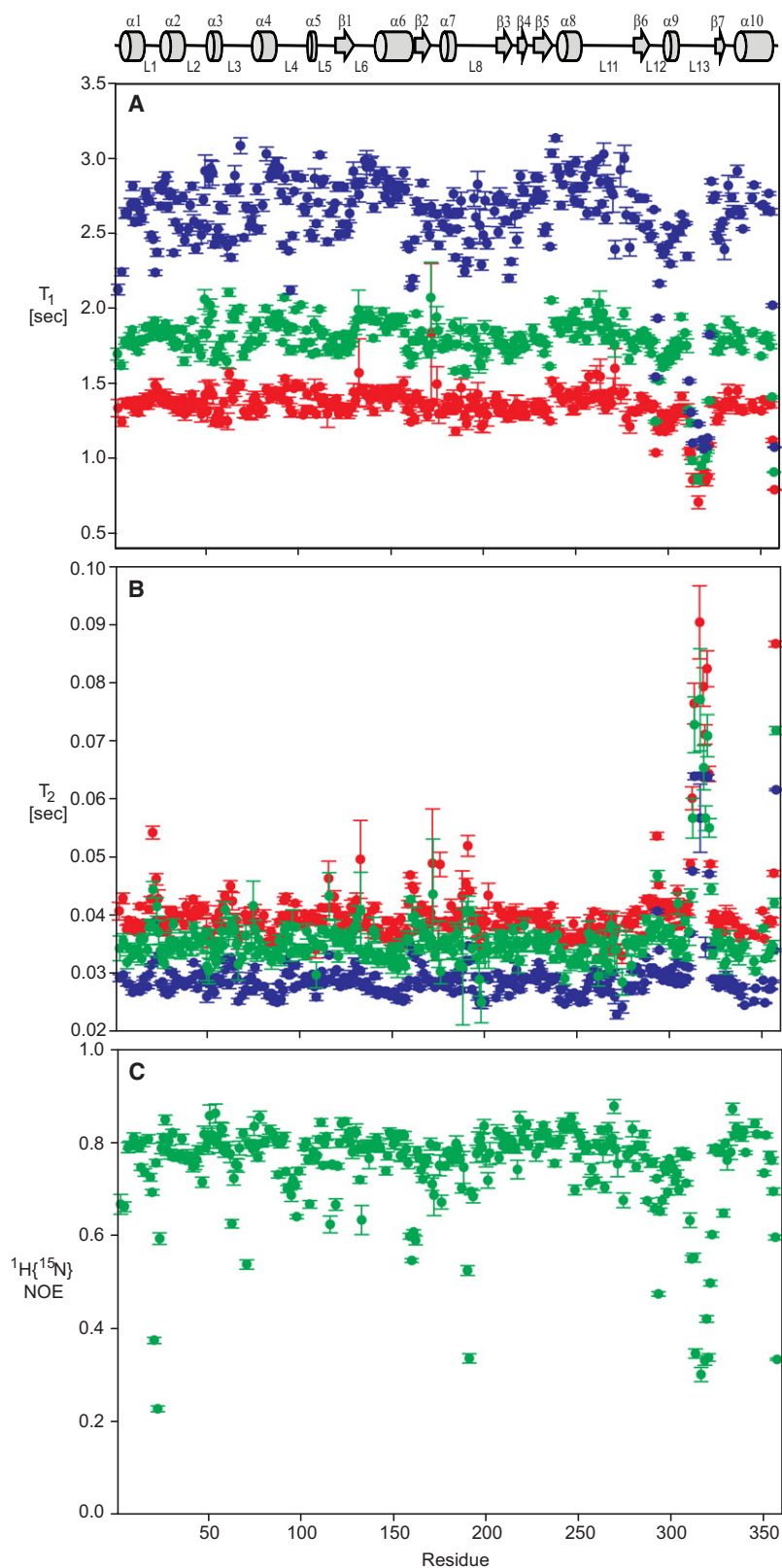


**Figure 5.  $^{15}\text{N}$  NMR Spin Relaxation Parameters of Substrate-Free Arginine Kinase**

Shown are  $T_1$  (A),  $T_2$  (B), and (c) $\{^1\text{H}\}^{15}\text{N}$  NOE (C) at  $^{15}\text{N}$  Larmor frequencies 50.65 (red), 60.78 (green), and 81.04 (blue). Individual values are listed in Table S1. Error bars on each measurement represent one standard deviation. The  $T_{1\text{rho}}$  spin lock time at 50.65 and 60.78 MHz was shorter than optimal for the slow relaxing amide signals in loop L13, resulting in relatively large errors. A schematic diagram of arginine kinase secondary structure is shown at the top with  $\alpha$  helices shown as cylinders,  $\beta$  strands as arrows, and loops and extended structure as lines.



**Table 2. Mean and Trimmed Mean  $^{15}\text{N}$   $T_1$ ,  $T_2$ , and Heteronuclear  $\{^1\text{H}\}^{15}\text{N}$  NOE Values for Backbone Amides of Arginine Kinase**

Parameter	50.65 MHz	60.78 MHz	81.04 MHz
$T_1$ [s]	$1.35 \pm 0.12$	$1.79 \pm 0.17$	$2.61 \pm 0.33$
Trimmed $T_1$ [s]	$1.36 \pm 0.06$	$1.82 \pm 0.09$	$2.69 \pm 0.16$
$T_2$ [s]	$0.041 \pm 0.007$	$0.036 \pm 0.006$	$0.029 \pm 0.005$
Trimmed $T_2$ [s]	$0.039 \pm 0.002$	$0.034 \pm 0.002$	$0.029 \pm 0.002$
Trimmed $T_1/T_2$	$35.34 \pm 3.25$	$53.08 \pm 5.00$	$96.46 \pm 9.49$
$\{^1\text{H}\}^{15}\text{N}$ NOE		$0.75 \pm 0.10$	
Trimmed $\{^1\text{H}\}^{15}\text{N}$ NOE		$0.79 \pm 0.04$	

Values are reported as the all-residue or trimmed mean  $\pm$  one standard deviation. Trimmed means are determined following criteria outlined in Tjandra et al. (1995b).  $\{^1\text{H}\}^{15}\text{N}$  NOE < 0.65 are excluded from trimmed  $\{^1\text{H}\}^{15}\text{N}$  NOE mean.

The primary structure of loop L8 is highly conserved across the phosphagen kinase family. Crystal structures of substrate-free mitochondrial creatine kinase and transition state analog form of muscle creatine kinase show an identical B factor pattern for the creatine kinase equivalent of loop L8 (Fritz-Wolf et al., 1996; Ohren et al., 2007). Furthermore, the results of hydrogen/deuterium exchange studies of creatine kinase are consistent with increased mobility in this loop (Mazon et al., 2004, 2005). These correlations between arginine kinase and creatine kinase suggest that the phosphagen kinase family of enzymes has evolved not only in structure, but also in dynamics of this and other catalytically important regions.

On the ns-ps timescale, loop L8, and the whole of dynamic domain 2, appears relatively rigid ( $S^2 = 0.85 \pm 0.03$ ) with the exception of three residues, E190, G191, and D192, located near but not at the loop tip, which have an  $S^2$  of 0.78, 0.73, and 0.78, respectively (Table S2 and Figure 4). Two of these residues, E190 and D192, exhibit measurable  $R_{\text{ex}}$  and also best fit model 5 ( $S^2_{\text{f}}$ ,  $S^2_{\text{s}}$ ,  $\tau_{\text{s}}$ ) and their NOEs are smaller than average (Table S2). This suggests a more complicated loop L8 motion.

#### Dynamics of Substrate Binding Loop L13 (V308–V322)

On the ns-ps timescale, the most prominent feature of motion in the enzyme is present in substrate binding loop L13, residues V308–V322 (Figures 5 and 6). Residues in the loop are best fit with model 5 ( $\tau_{\text{s}}$ ,  $S^2_{\text{s}}$ ,  $S^2_{\text{f}}$ ) resulting in a  $\tau_{\text{s}} \approx 1$  ns (Table 3). As noted above, use of a single  $\{^1\text{H}\}^{15}\text{N}$  NOE measurement limits the precision of the local correlation time constant. The average  $S^2$  is 0.53, substantially lower than average (Table S2). This increased flexibility is consistent with an absence of observable electron density for this region in the substrate-free arginine kinase crystal structure (Yousef et al., 2003). The correspondence of low order parameters and the absence of electron density suggest loop disorder is not an artifact of the crystalline state, since loop L13 becomes well ordered in the substrate-bound complex, with only slightly elevated B factors.

The conservation of elevated measures of thermal disorder in substrate-free crystal structures of phosphagen kinases from different *phyla* suggests a link to function. In substrate-bound arginine kinase, the side chains from two loop L13 residues directly contact substrate, R309 with nucleotide and E314 forming a salt link with substrate arginine (Zhou et al., 1998). R309 is

highly conserved in the phosphagen kinase family and E314 is less conserved, aligning with a valine in creatine kinases. An E314V mutant, in the context of swapping the arginine and creatine kinase loops, resulted in only 35% loss of activity, suggesting stabilization of the substrate-bound configuration involves interactions besides E314 (Azzi et al., 2004; Pruett et al., 2003). The structural, mutagenesis, and NMR studies suggest that the conserved primary structure of loop L13 across phosphagen kinases may reflect conservation of flexibility, as opposed to stabilization of substrate-bound state, as a necessary condition for catalysis.

#### Dynamics and Enzyme Catalysis

Through an increasing number of examples, it is becoming apparent that dynamics is important in the turnover of many enzymes (Boehr et al., 2006). General comments have been made about the slow turnover of phosphagen kinases being consistent with rate-limiting conformational change, but it is only now, with this work, that the specific mechanistic details are beginning to emerge. Particularly intriguing is the approximate correspondence between rate constants of conformational changes determined here by NMR ( $3\text{--}20\text{ s}^{-1}$ ) and the enzyme turnover rate ( $k_{\text{cat}} = 100\text{--}150\text{ s}^{-1}$ ) measured earlier by experimental kinetics, suggesting that conformational changes might be rate limiting on enzyme turnover. The two regions with motions at corresponding timescales are loop L8 and the NTD (or dynamic domain 1), which moves as a (quasi-)rigid group. It is possible that the intrinsic motions are in the same direction, if not of the same magnitude, as the changes seen between the substrate-free and -bound crystal structures, but the NMR analysis provides no direct evidence (Yousef et al., 2003; Zhou et al., 1998). The changes to loop L8 and the NTD contribute to the closing of the enzyme around the active site pocket. The most intriguing possibility is that turnover is gated by one or both of the motions. The difference between the slow rate constants of conformational exchange and turnover is not large and might be brought even closer if the presence of substrates modulates dynamics. It is also possible that substrate-associated changes to loop L8 and NTD were required and that evolutionary selection of residues that facilitate the conformational change could also have resulted in a loop that is intrinsically dynamic. In either case, it is possible that the ms timescale motions are part of an intrinsic conformational equilibrium whose populations are shifted by substrate binding toward a state required for reaction turnover (Boehr and Wright, 2008; Lange et al., 2008).

Loop L8 includes H185 that forms two interactions with the substrate nucleotide, stacking with the base and hydrogen bonding to the ribose (Zhou et al., 1998). While the rest of the loop is in the general area of the active site, this is the only direct interaction and it is not proximal to where bond breakage/formation is catalyzed. The same is true for the NTD, for which the only direct substrate interaction is between the substrate-specificity loop and the end of the phosphagen substrate that is remote from the reactive atoms. Thus, if intrinsic dynamics, observed by NMR, are rate limiting, their effects are exerted through substrate-binding or indirectly upon catalysis through propagated changes, rather than through direct influence on the catalytic chemistry.



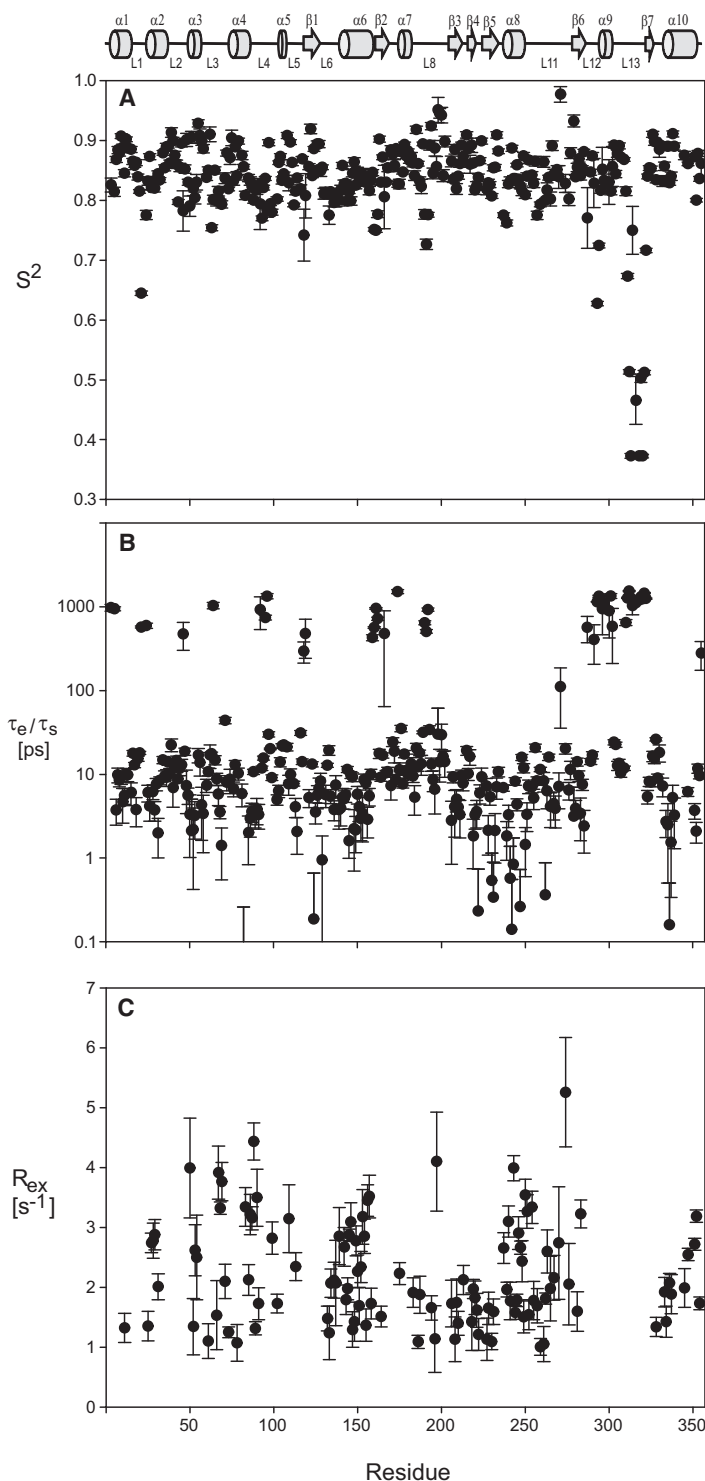


**Figure 6. Lipari-Szabo Model-Free Results for Substrate-Free Arginine Kinase Dynamics**

(A) Generalized order parameters.

(B)  $\tau_e/\tau_s$  internal time constants.

(C)  $R_{ex}$  at 600 MHz. All fit parameters and model selections are listed in Table S2. Errors were determined from Monte Carlo simulations.

turnover (Watt et al., 2007). The transition from a closed to an occluded conformation in dihydrofolate reductase, marked by a loop motion, has been shown to be rate limiting (Boehr et al., 2008). The motions in arginine kinase have analogs in these other systems. It is noteworthy that several motions are found together in arginine kinase: motion in a lid-like loop (L8), hinged domain motion (NTD), both of which are at turnover-commensurate rates, and the faster dynamics of loop L13 that folds over the active site. The presence of several modes of motions in arginine kinase, some of which might be turnover limiting, and the conservation of the dynamic structural elements adds to a growing awareness that conformational dynamics might be more widespread and functionally relevant to enzymes than has been heretofore widely appreciated.

## EXPERIMENTAL PROCEDURES

### Sample Preparation

Uniformly  $^{15}\text{N}$ -enriched and 80%  $^2\text{H}$ -enriched *Limulus polyphemus* arginine kinase was prepared as previously described (Davulcu et al., 2005). The final enzyme sample was concentrated to 1.0 mM in a buffer containing 10 mM sodium citrate (pH 6.5), 0.5 mM dithiothreitol, 50 mM potassium chloride, 50  $\mu\text{M}$  sodium azide, 90%  $\text{H}_2\text{O}$ , and 10%  $\text{D}_2\text{O}$ . Arginine kinase is stable for months at  $4^\circ\text{C}$  or  $20^\circ\text{C}$ , showing no signs of degradation or reduced enzymatic activity as judged by 2D [ $^{15}\text{N}$ ,  $^1\text{H}$ ] TROSY spectra and enzyme activity profiles over this same timescale (data not shown).

### NMR Spectroscopy

NMR data were recorded on Varian INOVA NMR spectrometers operating at  $^1\text{H}$  ( $^{15}\text{N}$ ) Larmor frequencies ( $\omega_0$ ) of 499.8(50.65), 599.7(60.78), 719.9(72.95), or 799.7(81.04) MHz. Each spectrometer was equipped with a HCN triple resonance probe and a z axis pulsed field gradient. All relaxation experiments were performed at  $25 \pm 0.5^\circ\text{C}$ , determined using a methanol standard (Raiford et al., 1979). Proton chemical shifts were referenced to the DSS methyl protons at 0 ppm and  $^{15}\text{N}$  chemical shifts referenced indirectly (Markley et al., 1998). Amide  $^1\text{H}$  and  $^{15}\text{N}$  resonance assignments of arginine kinase have been reported (Davulcu et al., 2005).

$^{15}\text{N}$   $T_1$  and heteronuclear [ $^1\text{H}$ ] $^{15}\text{N}$  NOE values were measured with relaxation experiments modified for TROSY detection (Farrow et al., 1994).  $T_{1\rho}$  was measured using relaxation experiments described in Korzhnev et al. (2002);  $T_2$  values were calculated from  $T_1$  and  $T_{1\rho}$  values. At 50.65 MHz,  $^{15}\text{N}$   $T_1$  was measured using relaxation delays of 0.151, 0.503\*, 1.006, 1.509, 2.012, and 3.017 s (asterisk denotes measurements duplicated for error estimation);  $^{15}\text{N}$   $T_{1\rho}$  was measured using relaxation delays of 5, 10\*, 25, 35, and 55 ms and a  $^{15}\text{N}$  spinlock field strength of 2.6 KHz. At 60.78 MHz,  $^{15}\text{N}$   $T_1$  was measured using relaxation delays of 0.151, 0.503\*, 1.006, 1.509, 2.012, and 4.5 s;  $^{15}\text{N}$   $T_{1\rho}$  was measured using relaxation delays of 5, 10\*, 25, 35, and 55 ms and a  $^{15}\text{N}$  spinlock field strength of 2.7 KHz. At 81.04 MHz,  $^{15}\text{N}$   $T_1$  was measured using relaxation delays of 0.151\*, 0.504, 1.010, 1.510, 2.010\*, 3.020, and 3.527 s;  $^{15}\text{N}$   $T_{1\rho}$  was measured using relaxation delays of 5\*, 15, 25\*, 35, and 55 ms and a  $^{15}\text{N}$  spinlock field strength of 2.7 KHz. The steady-state [ $^1\text{H}$ ] $^{15}\text{N}$  NOE was

The rate-limiting effect of protein dynamics on turnover has been shown for a number of other enzymes. Lid opening and closing has been shown to be rate limiting upon catalysis in, for example, adenylate kinase (Wolf-Watz et al., 2004) and triose phosphate isomerase (Rozovsky et al., 2001). A single histidine residue has been implicated in coupling motions in RNase A to

**Table 3. Summary of Lipari-Szabo Model Selection for Substrate-Free Arginine Kinase**

Model	Number of Residues	Percentage
1 ( $S^2$ )	5	1.7
2 ( $S^2$ , $\tau_e$ )	142	46.8
3 ( $S^2$ , $R_{ex}$ )	7	2.3
4 ( $S^2$ , $\tau_e$ , $R_{ex}$ )	106	35.0
5 ( $S^2_f$ , $S^2_s$ , $\tau_s$ )	43	14.2
Total	303	100.0

measured at 60.78 MHz using a  $^1\text{H}$  saturation time of 11 s (five times the longest  $^{15}\text{N}$   $T_1$ ).  $\{^1\text{H}\}^{15}\text{N}$  NOE was calculated from the intensity ratio of an experiment recorded with and without  $^1\text{H}$  saturation during the mixing time. Peak intensity error was estimated from the rms base plane noise and  $\{^1\text{H}\}^{15}\text{N}$  NOE error from propagation of error in quadrature.

Slow timescale chemical exchange was quantified using two different experimental NMR approaches. The first approach made use of constant relaxation time  $^{15}\text{N}$  spin CPMG relaxation dispersion with TROSY detection at three static fields,  $^{15}\text{N}$   $\omega_0 = 60.78$ , 72.95, and 81.04 MHz (Loria et al., 1999). In these experiments, the CPMG field strength ( $\nu$ ) is varied between 0 and 1 KHz by adjustment of the CPMG refocusing delay time. Data were recorded using the following parameters:  $^{15}\text{N}$   $\omega_0 = 60.78$  MHz, constant relaxation time = 40 ms,  $\nu = 0, 25, 50^*, 100, 200, 250, 300, 400, 500, 625, 750, 875$ , and 1000 Hz;  $^{15}\text{N}$   $\omega_0 = 72.95$  and 81.04 MHz, constant transverse relaxation time of 32 ms,  $\nu = 0^*, 31.25, 62.50, 93.75, 125^*, 156.25, 187.50, 250, 375, 500^*, 625^*, 750, 875$ , and 1000\* Hz. The second approach is based on measurement of  $^{15}\text{N}$  spin  $R_2^\beta$  (TROSY),  $R_2^\alpha$  (anti-TROSY) and longitudinal two-spin order  $R_1^{2\text{HzNz}}$  rate constants, which are then used to estimate  $R_{ex}$  (Wang et al., 2003).  $^{15}\text{N}$  spin  $R_2^\alpha$ ,  $R_2^\beta$ , and  $R_1^{2\text{HzNz}}$  experiments were recorded at  $^{15}\text{N}$   $\omega_0 = 60.78$  MHz. Experiments were recorded in duplicate at  $2\tau = 5/J_{\text{NH}}$  and, alternatively, the complete decay curves were recorded using relaxation time delays of  $2\tau = N/J_{\text{NH}}$  with  $N = 0, 1, 2^*, 3, 6$ , and 12 for  $R_2^\beta$ ;  $N = 0, 1^*, 2, 3$  for  $R_2^\alpha$ ;  $\tau = N/J_{\text{NH}}$  with  $N = 0, 1, 4^*, 10, 20$ , and 30 for  $R_1^{2\text{HzNz}}$ . Rate constants were taken from two parameter single exponential fits of peak intensities to relaxation delay times using the Levenberg-Marquardt algorithm.  $R_{ex}$  and  $\kappa$  were identical within measurement error, whether determined using a single  $2\tau = 5/J_{\text{NH}}$  relaxation time or by recording a full decay curve using multiple relaxation time increments.

All  $^{15}\text{N}$  spin relaxation data were recorded with  $\sim 100$  ms  $^1\text{H}$  acquisition time ( $t_{2\text{max}}$ ) and 75 ms  $^{15}\text{N}$  acquisition time ( $t_{1\text{max}}$ ) and processed with FELIX2004 to final matrices of  $4096 (^1\text{H}) \times 1024 (^{15}\text{N})$  points. Peak intensities were measured with SPARKY (Goddard and Kneller, 2008).  $^{15}\text{N}$  spin relaxation time constants  $T_1$  and  $T_{1\rho}$  were calculated from two-parameter single exponential fits of peak intensities to relaxation delay times using the Levenberg-Marquardt algorithm. The residual  $\chi^2$  values of the single exponential fits were generally less than or equal to the number of fit data points, suggesting the data were well fit.

### Slow ( $\mu\text{s}$ -ms) Time Scale Dynamics Analysis

Chemical exchange is a prevalent phenomenon in NMR spectroscopy and provides valuable information on kinetic processes occurring on the  $\mu\text{s}$ -ms timescale. It results from alternating an NMR spin between different magnetic environments, or chemical states. Arginine kinase residues experiencing  $\mu\text{s}$ -ms chemical exchange were identified using the method described in Wang et al. (2003) and using  $^{15}\text{N}$   $R_2$  relaxation dispersion (Loria et al., 1999). For those residues with  $R_{ex}$ , the former approach estimates the  $R_{ex}$  value, while the latter depends on analyzing the  $^{15}\text{N}$   $R_2$  rate constant as a function of effective CPMG field strength,  $\nu$ . Instead of recording a full relaxation decay curve at each CPMG field strength, a two-point  $^{15}\text{N}$   $R_2^{\text{eff}}$  is determined using a common reference experiment ( $I_0$ ) and a single intensity value ( $I_\nu$ ):  $R_2^{\text{eff}} = (-1/\tau_{\text{relax}}) \ln(I_\nu/I_0)$ , where  $\tau_{\text{relax}}$  is the constant relaxation time period. In the absence of chemical exchange,  $R_2^{\text{eff}}$  will be independent of  $\nu$ , while  $R_2^{\text{eff}}$  will vary with  $\nu$  in the presence of appropriate timescale chemical exchange. A plot of  $R_2^{\text{eff}}$  versus  $\nu$  generates a dispersion profile that can generally be fit to a simple, two site exchange model when  $\Delta R_2^{\text{eff}} = R_2^{\text{eff}}(\nu \rightarrow 0) - R_2^{\text{eff}}$

( $\nu = 1$  KHz)  $> 2$  s $^{-1}$ . Values below this threshold could not be reliably identified or fit. Arginine kinase residues with relaxation dispersion of this criteria were fit with a numerical approximation of the Bloch-McConnell equation using software kindly provided by L. Kay and D. Korzhnev (Cavanagh et al., 1996). In all cases, a two state exchange model was best-fit with the summed exchange rate constant  $k_{\text{ex}} = k_{\text{AB}} + k_{\text{BA}}$ , population of states A,  $p_A$ , and B,  $p_B$ , and their  $^{15}\text{N}$  chemical shift difference,  $\Delta\omega$ . No assumption was made regarding fast or slow exchange regime of  $k_{\text{ex}}$  relative to  $\Delta\omega$ .

### Fast Timescale Model-Free Analyses

The Lipari-Szabo simple model-free formalism describes protein dynamics with two timescales:  $\tau_m$  describes the rotational correlation time that reports on protein tumbling and  $\tau_e$  describes relative rapid internal motions (Lipari and Szabo, 1982a, 1982b). These motions are assumed to be decoupled from each other and typically exhibit a ratio ( $\tau_m/\tau_e$ ) greater than 10. Internal motions are described with the amplitude-dependent square of the generalized order parameter  $S^2$  and a ps-ns correlation time constant,  $\tau_e$ . This simple model has been extended to describe situations where fast,  $S^2_f$  and  $\tau_f$ , and slow,  $S^2_s$  and  $\tau_s$ , internal motions are present (Clore et al., 1990). The generalized order parameter describing this situation is expressed as the product  $S^2 = S^2_f S^2_s$ . Model-free analysis can also include an exchange term,  $R_{ex}$ , that adjusts the transverse relaxation rate constant to account for motions on the  $\mu\text{s}$ -ms timescale. The Lipari-Szabo spectral density functions are parameterized using a NH bond length of 1.04 Å and a  $^{15}\text{N}$  CSA of  $-170$  ppm.

Selection of the appropriate rotational diffusion model for substrate-free arginine kinase was established by considering the prediction of hydrodynamic behavior of the molecule based on structural coordinate using HYDRONMR (Garcia de la Torre et al., 2000) and by conducting an analysis of the  $\chi^2$  values derived from fits of the experimental NMR relaxation data using spectral density models for isotropic and axially symmetric rotational diffusion. Both diffusion models were parameterized with an identical subset of residues that does not contain contributions from motion on multiple timescales. The residues excluded were those with  $\{^1\text{H}\}^{15}\text{N}$  NOE  $< 0.75$ , those showing evidence of conformational exchange from  $T_1/T_2$  ratio analyses (Tjandra et al., 1995b), those with measured  $R_{ex}$ , and those not in regular secondary structure elements. Using these criteria, 136 residues were retained for use in parameterization in the diffusion models. The isotropic diffusion model was determined from a least-squares fit of the spectral density functions for  $T_1/T_2$  ratios to the experimental data as described. This calculation was performed with a subroutine in the software relxn2.2 with the rvi interface (Boyer and Lee, 2008). The axially symmetric diffusion model was parameterized from the crystal structure of substrate-free arginine kinase (PDB ID 1M80). This was accomplished by rotating the PDB coordinates to align the moments of inertia with the Cartesian axes and translated such that the enzyme center of mass was located at the origin. These manipulations were performed with PDBIN TERTIA provided by A.G. Palmer (Columbia University). Direction cosines of amide bond vectors in the alignment frame were determined using software from A.L. Lee (University of North Carolina).

The parameters  $S^2$ ,  $S^2_f$ ,  $S^2_s$ ,  $\tau_e$ ,  $\tau_s$ , and  $R_{ex}$  were fit to five standard motional models: model 1,  $S^2$  only; model 2,  $S^2$  and  $\tau_e$ ; model 3,  $S^2$  and  $R_{ex}$ ; model 4,  $S^2$ ,  $\tau_e$ , and  $R_{ex}$ ; and model 5,  $S^2_f$ ,  $S^2_s$ , and  $\tau_s$  using the model-selection subroutine of relxn2.2 (Boyer and Lee, 2008). Model selection for each residue was guided by the  $\chi^2$  statistic and the model with the lowest  $\chi^2$  was usually selected (d'Auvergne and Gooley, 2003). For residues in which  $R_{ex}$  was not observed in relaxation dispersion experiments, model 3 or 4 was only selected if the fit  $R_{ex}$  was greater than the experimental error on  $R_2$ , estimated as 1 s $^{-1}$ . Fits with  $\chi^2$  values  $> 150$  were not interpreted.

### SUPPLEMENTAL DATA

Supplemental Data include two tables and can be found with this article online at [http://www.cell.com/structure/supplemental/S0969-2126\(09\)00337-2](http://www.cell.com/structure/supplemental/S0969-2126(09)00337-2).

### ACKNOWLEDGMENTS

This research was supported by National Institutes of Health (GM77643; M.S.C.), the National Science Foundation through the National High Magnetic

Field Laboratory Institute for Health Research and Policy (DMR-0084173; J.J.S. and M.S.C.), and the American Heart Association (0415115B; O.D.).

Received: April 25, 2009

Revised: August 14, 2009

Accepted: August 15, 2009

Published: October 13, 2009

## REFERENCES

- Azzi, A., Clark, S.A., Ellington, W.R., and Chapman, M.S. (2004). The role of phosphagen specificity loops in arginine kinase. *Protein Sci.* **13**, 575–585.
- Beach, H., Cole, R., Gill, M.L., and Loria, J.P. (2005). Conservation of mus-mus enzyme motions in the apo- and substrate-mimicked state. *J. Am. Chem. Soc.* **127**, 9167–9176.
- Blethen, S.L. (1972). Kinetic properties of the arginine kinase isoenzymes of *Limulus polyphemus*. *Arch. Biochem. Biophys.* **149**, 244–251.
- Boehr, D.D., and Wright, P.E. (2008). Biochemistry. How do proteins interact? *Science* **320**, 1429–1430.
- Boehr, D.D., Dyson, H.J., and Wright, P.E. (2006). An NMR perspective on enzyme dynamics. *Chem. Rev.* **106**, 3055–3079.
- Boehr, D.D., Dyson, H.J., and Wright, P.E. (2008). Conformational relaxation following hydride transfer plays a limiting role in dihydrofolate reductase catalysis. *Biochemistry* **47**, 9227–9233.
- Bosshard, H.R. (2001). Molecular recognition by induced fit: how fit is the concept? *News Physiol. Sci.* **16**, 171–173.
- Boyer, J.A., and Lee, A.L. (2008). Monitoring aromatic picosecond to nanosecond dynamics in proteins via <sup>13</sup>C relaxation: expanding perturbation mapping of the rigidifying core mutation, V54A, in eglin c. *Biochemistry* **47**, 4876–4886.
- Cavanagh, J., Fairbrother, W.J., Palmer, A.G., III, and Skelton, A.J. (1996). *Protein NMR Spectroscopy* (San Diego: Academic Press).
- Clarkson, M.W., Gilmore, S.A., Edgell, M.H., and Lee, A.L. (2006). Dynamic coupling and allosteric behavior in a nonallosteric protein. *Biochemistry* **45**, 7693–7699.
- Clore, G.M., Szabo, A., Bax, A., Kay, L.E., Driscoll, P.C., and Gronenborn, A.M. (1990). Deviations from the simple two-parameter model-free approach to the interpretation of Nitrogen-15 nuclear magnetic relaxation of proteins. *J. Am. Chem. Soc.* **112**, 4989–4991.
- d'Auvergne, E.J., and Gooley, P.R. (2003). The use of model selection in the model-free analysis of protein dynamics. *J. Biomol. NMR* **25**, 25–39.
- Davulcu, O., Clark, S.A., Chapman, M.S., and Skalicky, J.J. (2005). Main chain (<sup>1</sup>H), (<sup>13</sup>C), and (<sup>15</sup>N) resonance assignments of the 42-kDa enzyme arginine kinase. *J. Biomol. NMR* **32**, 178.
- Dumas, C., and Janin, J. (1983). Conformational changes in arginine kinase upon ligand binding seen by small-angle X-ray scattering. *FEBS Lett.* **153**, 128–130.
- Ellington, W.R. (2001). Evolution and physiological roles of phosphagen systems. *Annu. Rev. Physiol.* **63**, 289–325.
- Farrow, N.A., Muhandiram, R., Singer, A.U., Pascal, S.M., Kay, C.M., Gish, G., Shoelson, S.E., Pawson, T., Forman-Kay, J.D., and Kay, L.E. (1994). Backbone dynamics of a free and phosphopeptide-complexed Src homology 2 domain studied by <sup>15</sup>N NMR relaxation. *Biochemistry* **33**, 5984–6003.
- Fritz-Wolf, K., Schnyder, T., Wallimann, T., and Kabsch, W. (1996). Structure of mitochondrial creatine kinase. *Nature* **381**, 341–345.
- Furter, R., Furter-Graves, E.M., and Wallimann, T. (1993). Creatine kinase: the reactive cysteine is required for synergism but is nonessential for catalysis. *Biochemistry* **32**, 7022–7029.
- Garcia de la Torre, J., Huertas, M.L., and Carrasco, B. (2000). HYDRONMR: prediction of NMR relaxation of globular proteins from atomic-level structures and hydrodynamic calculations. *J. Magn. Reson.* **147**, 138–146.
- Gattis, J.L., Ruben, E., Fenley, M.O., Ellington, W.R., and Chapman, M.S. (2004). The active site cysteine of arginine kinase: structural and functional analysis of partially active mutants. *Biochemistry* **43**, 8680–8689.
- Gerstein, M., Lesk, A.M., and Chothia, C. (1994). Structural mechanisms for domain movements in proteins. *Biochemistry* **33**, 6739–6749.
- Goddard, T.D., and Kneller, D.G. (2008). SPARKY 3 (<http://www.cgl.ucsf.edu/home/sparky/>).
- Hayward, S. (1999). Structural principles governing domain motions in proteins. *Proteins* **36**, 425–435.
- Hayward, S., and Berendsen, H.J. (1998). Systematic analysis of domain motions in proteins from conformational change: new results on citrate synthase and T4 lysozyme. *Proteins* **30**, 144–154.
- Jencks, W.P. (1969). *Catalysis in Chemistry and Enzymology* (New York: McGraw-Hill).
- Jencks, W.P. (1975). Binding energy, specificity, and enzymic catalysis: the circe effect. *Adv. Enzymol. Relat. Areas Mol. Biol.* **43**, 219–410.
- Jencks, W.P., and Mage, M.I. (1974). "Orbital steering", entropy, and rate accelerations. *Biochem. Biophys. Res. Commun.* **57**, 887–892.
- Korzhev, D.M., Skrynnikov, N.R., Millet, O., Torchia, D.A., and Kay, L.E. (2002). An NMR experiment for the accurate measurement of heteronuclear spin-lock relaxation rates. *J. Am. Chem. Soc.* **124**, 10743–10753.
- Koshland, D.E., Jr. (1958). Application of a theory of enzyme specificity to protein synthesis. *Proc. Natl. Acad. Sci. USA* **44**, 98–104.
- Koshland, D.E., Jr. (1994). The key-lock theory and the induced-fit theory. *Angew. Chem. Int. Ed. Engl.* **33**, 2375–2378.
- Kovrig, E.L., and Loria, J.P. (2006). Enzyme dynamics along the reaction coordinate: critical role of a conserved residue. *Biochemistry* **45**, 2636–2647.
- Lahiri, S.D., Wang, P.F., Babbitt, P.C., McLeish, M.J., Kenyon, G.L., and Allen, K.N. (2002). The 2.1 Å structure of *Torpedo californica* creatine kinase complexed with the ADP-Mg<sup>2+</sup>-NO<sub>3</sub><sup>-</sup>-creatine transition-state analogue complex. *Biochemistry* **41**, 13861–13867.
- Lange, O.F., Lakomek, N.A., Fares, C., Schroder, G.F., Walter, K.F., Becker, S., Meiler, J., Grubmuller, H., Griesinger, C., and de Groot, B.L. (2008). Recognition dynamics up to microseconds revealed from an RDC-derived ubiquitin ensemble in solution. *Science* **320**, 1471–1475.
- Lee, R.A., Razaz, M., and Hayward, S. (2003). The DynDom database of protein domain motions. *Bioinformatics* **19**, 1290–1291.
- Lipari, G., and Szabo, A. (1982a). Model-free approach to the interpretation of nuclear magnetic resonance relaxation in macromolecules. 1. Theory and range of validity. *J. Am. Chem. Soc.* **104**, 4546–4559.
- Lipari, G., and Szabo, A. (1982b). Model-free approach to the interpretation of nuclear magnetic resonance relaxation in macromolecules. 2. Analysis of experimental results. *J. Am. Chem. Soc.* **104**, 4559–4570.
- Loria, J.P., Rance, M., and Palmer, A.G., 3rd. (1999). A TROSY CPMG sequence for characterizing chemical exchange in large proteins. *J. Biomol. NMR* **15**, 151–155.
- Ma, B., Kumar, S., Tsai, C.J., and Nussinov, R. (1999). Folding funnels and binding mechanisms. *Protein Eng.* **12**, 713–720.
- Mandel, A.M., Akke, M., and Palmer, A.G., 3rd. (1995). Backbone dynamics of *Escherichia coli* ribonuclease HI: correlations with structure and function in an active enzyme. *J. Mol. Biol.* **246**, 144–163.
- Markley, J.L., Bax, A., Arata, Y., Hilbers, C.W., Kaptein, R., Sykes, B.D., Wright, P.E., and Wuthrich, K. (1998). Recommendations for the presentation of NMR structures of proteins and nucleic acids. IUPAC-IUBMB-IUPAB Inter-Union Task Group on the Standardization of Data Bases of Protein and Nucleic Acid Structures Determined by NMR Spectroscopy. *J. Biomol. NMR* **12**, 1–23.
- Mazon, H., Marcillat, O., Forest, E., Smith, D.L., and Vial, C. (2004). Conformational dynamics of the GdmHCl-induced molten globule state of creatine kinase monitored by hydrogen exchange and mass spectrometry. *Biochemistry* **43**, 5045–5054.
- Mazon, H., Marcillat, O., Forest, E., and Vial, C. (2005). Local dynamics measured by hydrogen/deuterium exchange and mass spectrometry of creatine kinase digested by two proteases. *Biochimie* **87**, 1101–1110.
- Ohren, J.F., Kundracik, M.L., Borders, C.L., Jr., Edmiston, P., and Viola, R.E. (2007). Structural asymmetry and intersubunit communication in muscle creatine kinase. *Acta Crystallogr. D Biol. Crystallogr.* **63**, 381–389.

- Osborne, M.J., Schnell, J., Benkovic, S.J., Dyson, H.J., and Wright, P.E. (2001). Backbone dynamics in dihydrofolate reductase complexes: role of loop flexibility in the catalytic mechanism. *Biochemistry* *40*, 9846–9859.
- Palmer, A.G., 3rd, Kroenke, C.D., and Loria, J.P. (2001). Nuclear magnetic resonance methods for quantifying microsecond-to-millisecond motions in biological macromolecules. *Methods Enzymol.* *339*, 204–238.
- Pruett, P.S., Azzi, A., Clark, S.A., Yousef, M., Gattis, J.L., Somasundaram, T., Ellington, W.R., and Chapman, M.S. (2003). The putative catalytic bases have, at most, an accessory role in the mechanism of arginine kinase. *J. Biol. Chem.* *278*, 26952–26957.
- Raiford, D.S., Fisk, C.L., and Becker, E.D. (1979). Calibration of methanol and ethylene glycol nuclear magnetic resonance thermometers. *Anal. Chem.* *51*, 2050–2051.
- Rozovsky, S., Jogl, G., Tong, L., and McDermott, A.E. (2001). Solution-state nmr investigations of triosephosphate isomerase active site loop motion: ligand release in relation to active site loop dynamics. *J. Mol. Biol.* *310*, 271–280.
- Sullivan, S.M., and Holyoak, T. (2008). Enzymes with lid-gated active sites must operate by an induced fit mechanism instead of conformational selection. *Proc. Natl. Acad. Sci. USA* *105*, 13829–13834.
- Suzuki, T., Kawasaki, Y., Furukohri, T., and Ellington, W.R. (1997). Evolution of phosphagen kinase. VI. Isolation, characterization and cDNA-derived amino acid sequence of lombricine kinase from the earthworm *Eisenia foetida*, and identification of a possible candidate for the guanidine substrate recognition site. *Biochim. Biophys. Acta* *1343*, 152–159.
- Tjandra, N., Feller, S.E., Pastor, R.W., and Bax, A. (1995a). Rotational diffusion anisotropy of human ubiquitin from 15N NMR relaxation. *J. Am. Chem. Soc.* *117*, 12562–12566.
- Tjandra, N., Kuboniwa, H., Ren, H., and Bax, A. (1995b). Rotational dynamics of calcium-free calmodulin studied by 15N-NMR relaxation measurements. *Eur. J. Biochem.* *230*, 1014–1024.
- Vugmeyster, L., Raleigh, D.P., Palmer, A.G., 3rd, and Vugmeister, B.E. (2003). Beyond the decoupling approximation in the model free approach for the interpretation of NMR relaxation of macromolecules in solution. *J. Am. Chem. Soc.* *125*, 8400–8404.
- Wang, C., Rance, M., and Palmer, A.G., 3rd. (2003). Mapping chemical exchange in proteins with MW > 50 kD. *J. Am. Chem. Soc.* *125*, 8968–8969.
- Wang, C., Karpowich, N., Hunt, J.F., Rance, M., and Palmer, A.G. (2004). Dynamics of ATP-binding cassette contribute to allosteric control, nucleotide binding and energy transduction in ABC transporters. *J. Mol. Biol.* *342*, 525–537.
- Watt, E.D., Shimada, H., Kovrigin, E.L., and Loria, J.P. (2007). The mechanism of rate-limiting motions in enzyme function. *Proc. Natl. Acad. Sci. USA* *104*, 11981–11986.
- Wolf-Watz, M., Thai, V., Henzler-Wildman, K., Hadjipavlou, G., Eisenmesser, E.Z., and Kern, D. (2004). Linkage between dynamics and catalysis in a thermophilic-mesophilic enzyme pair. *Nat. Struct. Mol. Biol.* *11*, 945–949.
- Yousef, M.S., Fabiola, F., Gattis, J., Somasundaram, T., and Chapman, M.S. (2002). Refinement of arginine kinase transition-state analogue complex at 1.2 Å resolution: mechanistic insights. *Acta Crystallogr. D Biol. Crystallogr.* *58*, 2009–2017.
- Yousef, M.S., Clark, S.A., Pruet, P.K., Somasundaram, T., Ellington, W.R., and Chapman, M.S. (2003). Induced fit in guanidino kinases—comparison of substrate-free and transition state analog structures of arginine kinase. *Protein Sci.* *12*, 103–111.
- Zhou, G., Somasundaram, T., Blanc, E., Parthasarathy, G., Ellington, W.R., and Chapman, M.S. (1998). Transition state structure of arginine kinase: implications for catalysis of bimolecular reactions. *Proc. Natl. Acad. Sci. USA* *95*, 8449–8454.